Astron. Astrophys. 319, 250–259 (1997)

ASTRONOMY AND ASTROPHYSICS

Fractionated stellar wind – the example of σ Orionis E

D. Groote[1] **and K. Hunger**[2]

[1] Hamburger Sternwarte, Gojenbergsweg 112, D-21029 Hamburg, Germany
[2] Institut für Astronomie und Astrophysik, Universität Kiel, Leibnizstraße, Physikzentrum, D-24098 Kiel, Germany

Received 23 December 1995 / Accepted 6 July 1996

Abstract. In main-sequence stars, at effective temperatures below $\simeq$ 20 000 K, radiation ceases to be able to drive a stellar wind. In a rather narrow transition regime, elemental segregation seems possible due to the decoupling of He and, under special circumstances, also of H from the absorbing metal ions in the wind. This effect may even be more pronounced, if the wind is surface modulated, say by a magnetic field and rotation.

A first example of the latter kind is shown to be the He-variable HD 37479 (σ Ori E) which has two axes of symmetry, one characterized by the depletion of metals and one by the enrichment of He. The former is oriented along the magnetic dipole axis, while the latter is set off by roughly 45°. Theory of diffusion is unable to explain these symmetries.

In order to locate the the wind bases, phase variations of the wind are extracted from IUE-spectrograms. It is shown that there exist two wind modes: a weak and variable inner (photospheric) wind that feeds the corotating clouds, and a phase independent outer (coronal) wind which has its origin in a hot corona outside the clouds.

The resulting phase variations of the photospheric wind are in good agreement with the predictions of a semi-quantitative wind model. The wind bases further turn out to be (practically) congruent with the observed He-patches. Hence it is concluded that the surface enrichment of He indeed is due to decoupling of He from the metals in the wind. The metal poor polar caps, however, cannot be explained in this way. H-decoupling, evidently, does not play a role in σ Ori E. Instead, arguments are brought forward that point to accretion caps on top of the magnetic poles, possibly of reaccreted H (and He) that veils the UV-metal lines. σ Ori E appears to be the first stellar object with a fractionated wind, i.e. a wind whose chemical composition is distinctly different from the composition of its base.

Key words: stars: atmospheres – stars: chemically peculiar – stars: circumstellar matter – stars: individual: HD37479(σ Ori E) – stars: magnetic field – stars: mass loss

Send offprint requests to: K. Hunger, e: mail (D. Groote): dgroote@hs.uni-hamburg.de

1. Introduction

For main sequence stars with $T_{\rm eff} \lesssim$ 20 000 K, $\dot{M}$ rapidly drops to small values with decreasing temperatures, as radiation ceases to be able to drive the wind (Abbott 1982, Babel 1995). At these temperatures the density of the wind decreases and the coupling via collisions between the metal ions which absorb the photons and H and He (passive plasma) becomes weak, with the result that (the singly ionized) He decouples (Springmann & Pauldrach 1992), and at somewhat lower temperatures, possibly also H. So with decreasing effective temperature, a star with otherwise solar composition may thus have a He-rich, or under special circumstances a metal poor photosphere.

The critical temperature range is anticipated to be narrow, so that the chance to detect stars with such abundance anomalies may be small. However, if the wind is surface modulated as e.g. in a rotating and magnetized star, the chance to discover a star with these anomalies is much greater. The oblique rotator HD 37479 (σ Ori E) may be a good example.

σ Ori E is the best studied variable B_p star. Observations comprise most of the accessible electro magnetic spectrum, from X-ray to radio. Observations include spectroscopy, photometry, magnetometry and polarisation (see e.g. Groote & Hunger 1976, Pedersen 1979, Shore & Adelman 1981, Barker et al. 1982, Bohlender 1988, Walborn & Hesser 1976, Hesser et al. 1977, Landstreet & Borra 1978, Bohlender et al. 1987, Kemp & Herman 1977, Drake et al. 1987, Berghöfer & Schmitt 1994.) Most of the observed quantities are variable, with a common period of P = 1.19 d. A model that matches all observations is schematically shown in Fig. 1. It represents an oblique rotator with two corotating clouds, two He-rich patches and two metal poor caps, centered at the magnetic poles (see e.g. Hunger & Groote 1982).

The uncomfortable situation is that we have an empirical model that is well based on a large array of phase covering observations, but are unable to explain its main features, namely the local enrichment of He at intermediate magnetic latitudes and the polar depletion of metals. Diffusion to be operative requires that the stellar wind $\dot{M}$ does not exceed $10^{-13}{\rm M}_\odot{\rm yr}^{-1}$ (Michaud 1992). However, $\dot{M} \approx 10^{-10} - 10^{-9}{\rm M}_\odot{\rm yr}^{-1}$ is inferred from observations (Hamann 1981, see discussion be-

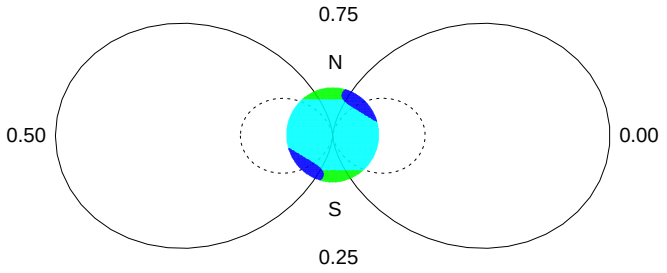

Fig. 1. Schematic model of σ Ori E (seen rotational pole-on): Two clouds trapped within closed magnetic field lines are forced into corotation. For simplicity, a centered dipole with $\beta = 90°$ is here assumed. At both magnetic poles metal-poor caps, and offset by $\approx 45°$, two He-patches are visible. Phases are indicated by numbers. The inner (dashed) and outer (full drawn) lines are supposed to contain the corotating clouds.

low), and also from theory (Pauldrach 1989). And even if diffusion processes were operative(i.e. in a sufficiently weak wind), He should accumulate in circumpolar or in equatorial bands (Michaud et al. 1987), depending on the mass loss rate, while it may accumulate at the magnetic poles in the region of the first ionization of He (Vauclair et. al 1991). Likewise the depletion of metals at the magnetic poles is not explained by diffusion. It must also be noted that the depletion of metals occurs for all ions studied (C IV, Si IV, Al III, Fe III), irrespectively of e/m, state of ionization, and excitation (Hunger et al. 1990). Since the effective temperature of σ Ori E ($T_{\rm eff}$ = 22 500 K) falls close to the above mentioned critical range, it appears worthwhile to test whether elemental segregation due to the decoupling of He, and possibly also of H, in the wind may lead to the observed surface distribution. Since the decoupling of He, and possibly also of H ("run away effect"), essentially will lead to the (initial) removal of the elements in question from the wind, we henceforth call this separation mechanism "fractionation", in analogy to the process of fractionated evaporation.

To this end, the surface distribution of the wind will be derived from the phase variations of C IV 1548, 1551 and Si IV 1394, 1403 as extracted from 35 phase covering, high resolution IUE spectrograms (IUE archives). The data reduction is described in Sect. 2. Two wind components are required by the observations: a phase independent ("coronal") wind and a phase variable ("photospheric") wind which will be discussed in Sect. 2. An attempt is made to separate the two components. A semi-quantitative theory of the photospheric wind is outlined in Sect. 3. Its aim is to define the wind bases on the surface of a rotating and magnetized star. As observations and "theory" yield consistent results, and as the bases of the photospheric winds turn out to be (practically) congruent with the He patches, it is concluded that the He-enrichment indeed occurs at the bases of the photospheric wind. The wind scenario, however, is unable to explain the metal deficiencies. An alternative scenario is discussed (Sect. 4). Model calculations and surface mapping are presented in Sect. 5 in order to check whether the new concept of He-segregation yields results that are free of contradictions.

Table 1. Short wavelength high-resolution IUE-spectra of σ Ori E with phases, wavelength shift (pixels), and image number

Φ	shift	image #	Φ	shift	image #
0.058	-2	7560	0.512	-2	15757
0.075	1	7529	0.550	-2	15759
0.120	-2	15778	0.577	-2	7587
0.160	0	15780	0.587	3	4840
0.199	0	15782	0.590	-2	15811
0.210	-1	7607	0.628	-2	15813
0.254	2	7532	0.659	-2	7589
0.279	-1	7609	0.668	-2	15815
0.297	-4	2230	0.706	-2	15817
0.327	-4	2231	0.742	0	7553
0.350	0	7534	0.823	-1	7555
0.378	0	7583	0.831	0	3522
0.395	-1	15751	0.839	0	15785
0.422	-2	3539	0.860	0	15786
0.436	-1	15753	0.866	-1	7556
0.446	0	7536	0.880	0	15787
0.475	-2	15755	0.951	-1	7558
0.483	-1	7537			

In Sect. 6, results will be discussed and in Sect. 7, conclusions are drawn.

2. Reduction of IUE data and wind profiles

The wind is discussed on the basis of 35 high resolution spectrograms (see Table 1) covering well all phases were obtained from the IUE archives. (Phase calculations correspond to Hesser et al. 1977.) Since the signal-to-noise ratio is poor, and the spectrum crowded with blends, some efforts are needed to extract reliable profiles and equivalent widths. The procedure goes briefly as follows: For each order, at the central wavelength, the continuum is defined. To all these points, splines are adapted that describe the march of the continuum. The actual spectrograms are then normalized to unity, by division. After rectification, the wavelength scale is corrected, using interstellar absorption lines (corrections are $\leqq 4$ pixels, see Table 1). To obtain a high S/N reference spectrum, the spectrograms of all phases are coadded, weighted with the individual signal-to-noise ratios. Finally, from the individual spectrum, the phase averaged spectrum is subtracted, a procedure that simplifies greatly the detection of phase variations. The *individual* spectrum in many cases will also be binned using adjacent phases (3-5 typically) which do not exceed the desired time resolution ($\Delta\Phi \leqq 0.05$).

2.1. Coronal wind

Fig. 2 shows as an example the profiles of C IV 1548, 1551 at phase Φ = 0.36 (binned from 0.327 to 0.395, full drawn). The mean of all 35 profiles is dotted. The profile of C IV 1548 is asymmetric, with the blue absorption extending to -600 km s^{-1}. (This asymmetry does not show up for C IV 1551 at the metal rich phase Φ = 0.36 as the blue wing is blended with

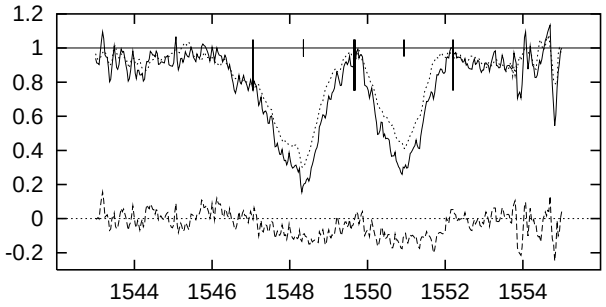

Fig. 2. Profiles of C IV 1548, 1551 at phase $\Phi = 0.36$ (full drawn) and mean of all spectra (dotted). The difference spectrum is included (dashed), vertical tick marks indicate integration intervals and line centers.

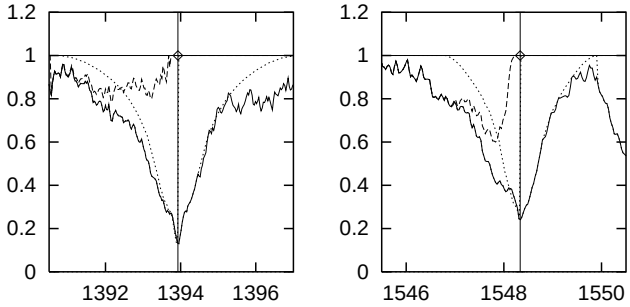

Fig. 3. Coronal wind profiles of Si IV 1394 (left) and C IV 1548 (right). Mean profiles (full drawn), adopted line profiles (dotted) and extracted wind profiles (dashed).

Fe III lines.) In the difference profile (bottom), the asymmetry vanishes. The difference spectrum, hence, reflects the difference of the photospheric abundances between the phase $\Phi = 0.36$ and phase average. In the present case, the difference is negative. A similar result is obtained for all other phases (not shown for lack of space), as well for C IV 1548, 1551 as for Si IV 1394, 1403, except for minor variations that will be discussed in Sect. 2.2. Hence it must be concluded that the wind is largely phase independent, a result that can only mean that the major component of the wind has its origin outside the magnetosphere (clouds), as otherwise the (decentered) dipole field would have modulated the wind. This component is termed *coronal*[1] (see Sect. 6). The coronal wind profile is obtained in the usual manner: The blue wing of the mean profile is divided by its red wing (see Fig. 3, here we used a smoothed and corrected half profile). The 0.2 Å range near the central wavelength is set to zero to suppress the large scatter due to binning effects from the interstellar component. The equivalent widths are $W_\lambda \approx 0.5$ Å for C IV 1548 and $W_\lambda \approx 0.4$ Å for Si IV 1394. The extracted wind profiles for the two elements look different, as it may be expected due to different excitation conditions. It is essentially the coronal wind that in the past has been used to determine the mass loss rate of σ Ori E (Hamann 1981), see below.

2.2. Photospheric wind

Steady state solution requires that there is an inner (photospheric) wind that feeds the clouds at the same rate as mass is lost from the clouds via the coronal wind (see also Havnes & Goertz 1984). Since σ Ori E rotates with $P = 1.19$ d and has a strong (decentered) dipole field (which is inclined with respect to the axis of rotation), the photospheric wind is expected to be phase modulated. As the main wind feature is essentially constant, with $W_{\lambda\,1548} \approx 0.5$ Å, the photospheric wind can have only a small amplitude, not exceeding $W_{\lambda\,1548} \approx 0.1$ Å. In order to detect such small variations, the following procedure has been worked out: at each phase, the difference profile (see above) is formed. In this way the contribution of the coronal wind is eliminated. Then truncated half equivalent widths are obtained, by integrating from -1.5 - 0 Å$\rightarrow$ $W^-_{\lambda/2}$, and 0 - 1.5 Å$\rightarrow$ $W^+_{\lambda/2}$ (in Fig. 2, integration intervals are denoted by tick marks). In phases with wind, $\Delta W_{\lambda/2} = W^-_{\lambda/2} - W^+_{\lambda/2} > 0$, otherwise zero.[2]

In Fig. 4a, $W^-_{\lambda/2}$ (full drawn) and $W^+_{\lambda/2}$ (dashed) are shown for Si IV 1394, as function of phase. The sum $W^-_{\lambda/2}$+$W^+_{\lambda/2}$ illustrates the march of W_λ, with its minima near the magnetic poles ($\Phi_N = 0.75, \Phi_S = 0.21$). At most phases, the difference $\Delta W_{\lambda/2}$ is small. Two maxima with $\Delta W_{\lambda/2} \approx 0.1$ Å show up near $\Phi = 0.3$ and 0.85. [3] The other three UV resonance lines Si IV 1403, C IV 1548 and 1551 yield the same result (Fig. 4b–d). As a null test, the subordinate line C II 1324 which is anticipated to be formed in the photosphere has been evaluated in the same manner. It does not exhibit a blue wind component, and as it lies mostly on the flat part of the curve of growth, no photospheric variations are expected. $\Delta W_{\lambda/2}$ indeed does not differ significantly from zero (Fig. 4e).

According to Fig. 4a–d, the centers of the photospheric wind base appear at phases $\Phi = 0.3$ and 0.85, i.e. at an angular distance of about 30° from the nearest pole. This distance can also be obtained from the radial distribution of the clouds. The latter extend from 2 - 5 stellar radii (Hunger et al. 1989). Taking the mean $\bar{r} = 3\,r_\star$ and assuming that the cloud matter is bound to the dipole field lines then one can trace back their origin on the stellar surface, which yields the same angular distance as before.

The profiles of the photospheric wind can be obtained only with an order of magnitude accuracy. This is done in two steps. First the coronal wind is eliminated from the line profiles of the phase where the wind is found to be at its maximum $\Phi = 0.85$

[1] Corona in this context must not be confused with the solar type corona. Here it defines the hot circumstellar region outside the rotating magnetosphere.

[2] Radial velocity shifts may also occur due to the non-uniform surface distribution of the metals. These effects, however, are small (see Sect. 6).

[3] $\Delta W_{\lambda/2} \approx 0.1$ Å corresponds to the small value of 2σ (single spectrogram). However, one has to consider that there are 2-3 spectra at phases $\Phi = 0.3$, and 6 spectra at $\Phi = 0.85$ which do exhibit this difference. Furthermore there are 4 different spectral lines which yield the same results.

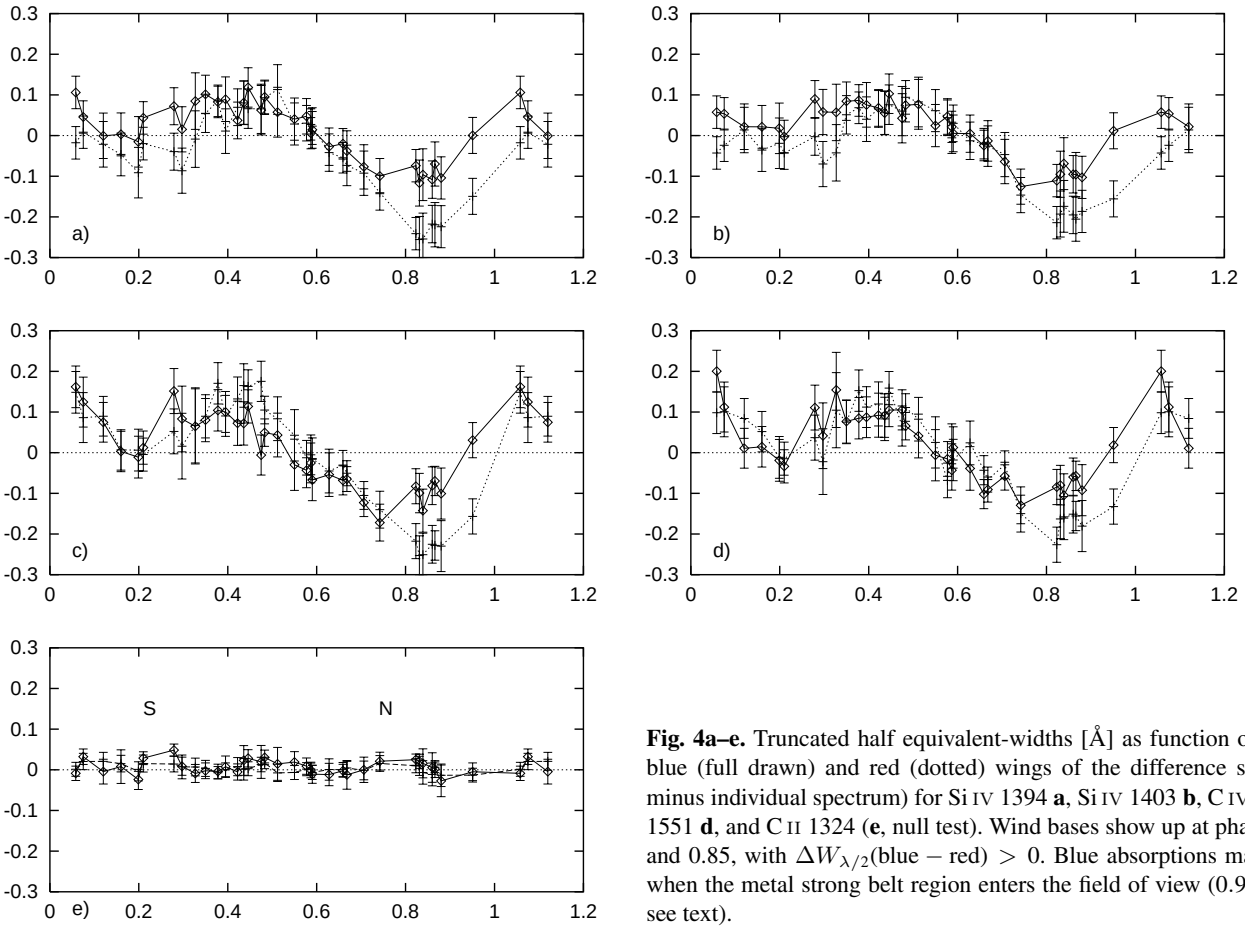

Fig. 4a–e. Truncated half equivalent-widths [Å] as function of phase Φ of blue (full drawn) and red (dotted) wings of the difference spectra (mean minus individual spectrum) for Si IV 1394 **a**, Si IV 1403 **b**, C IV 1548 **c**, C IV 1551 **d**, and C II 1324 (**e**, null test). Wind bases show up at phases Φ = 0.29 and 0.85, with $\Delta W_{\lambda/2}$(blue − red) $>$ 0. Blue absorptions may also occur when the metal strong belt region enters the field of view ($0.9 < \Phi < 1.0$, see text).

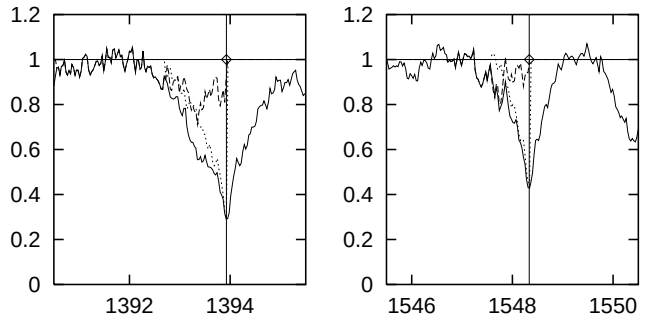

Fig. 5. Same as Fig. 3 for the extraction of the photospheric wind profiles. Net profiles (full drawn, coronal wind eliminated) for phase Φ = 0.85, mirrored red wings (dotted), and photospheric wind profiles (dashed, see text).

(binned from $\Phi = 0.823 - 0.880$), by division with a phase averaged profile. Then as before the blue wing of the net profile is divided by its red wing. The profiles are shown in Fig. 5 for Si IV 1394 and C IV 1548. In Fig. 6 all wind profiles (coronal and photospheric) are shown as function of R.V.. On account of the large scatter, the photospheric wind profiles may be meaningless. The equivalent widths, however, yield the expected order of magnitude (0.1 Å for C IV 1548), i.e. of roughly 20% of the coronal wind.

3. The photospheric wind - a theoretical approach

A full theoretical description of a stellar wind in the atmosphere of a rotating and magnetized star is beyond the scope of the present paper. It would entail the discussion of the radiative acceleration of a 3 component plasma (H, He, metals), Lorentzian forces, and inertial forces. Instead, we pursue a simple semi-quantitative approach which yields results that may not be too far from reality.

We consider two stars: the first star having a B-field, but without rotation. If the B-field is strong, the trajectories of the wind particles follow the field lines (in this example a centered dipole, and the magnetic obliquity β set to 90°): trajectory 1. For the second star we assume that there is no B-field but rotation. Wind trajectories of the latter can be obtained by adopting a velocity field – in our case it is taken from Kudritzki et al. (1989), as computed by Pauldrach (1989) for the case of σ Ori E, neglecting rotation and magnetic fields: trajectory 2.

Now in the case of a rotating and magnetized star, the wind can only freely develop if trajectory 1 is equal to trajectory 2, as in that case no Lorentzian forces will be induced by the rotation (see Fig. 7). This in general will not be possible: trajectories will intersect and thus wind particles are forced to move in Larmor circles, depending on the angle δ between the two trajectories. This means that kinetic energy of (outward) translation is partly

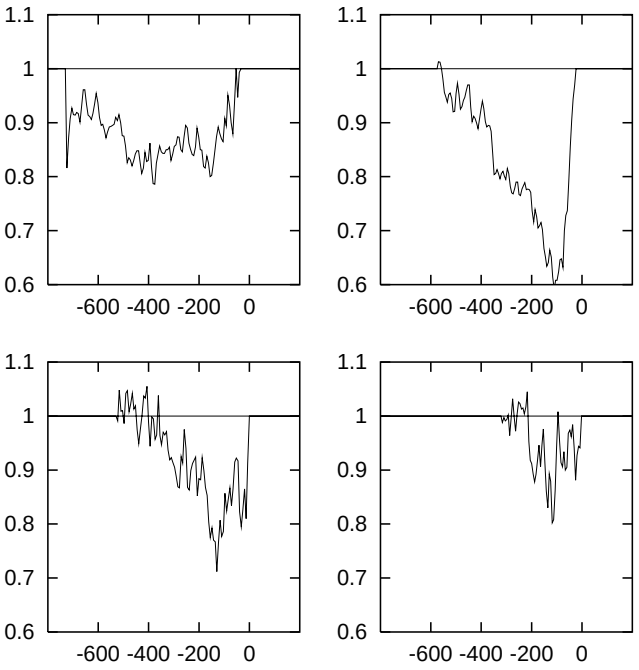

Fig. 6. Coronal (top) and photospheric (bottom) wind profiles (see Figs. 3 and 5) for Si IV 1394 (left) and C IV 1548 (right) as function of R.V. [km s^{-1}].

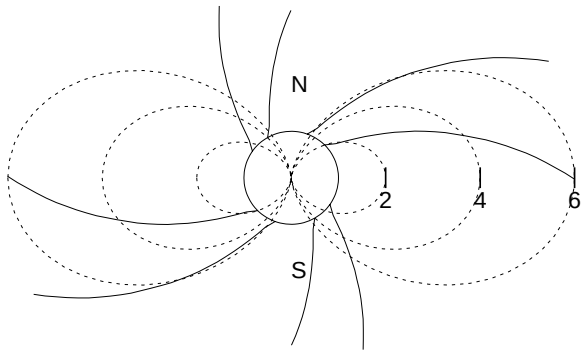

Fig. 7. Wind trajectories in the (rotational) equatorial plane: trajectories 1 dotted, trajectories 2 full drawn. Stellar distances are indicated by numbers.

redistributed into kinetic energy of rotation, thereby eventually braking the wind. But for a given star, there may be selected surface regions where the two trajectories intersect at small angles, i.e. where the interactions are smaller than at other regions. Instead of comparing the trajectories from the stellar surface out to the clouds, we choose a reference sphere somewhat larger than the star itself, at which we calculate the Larmor frequency ω_L arising from the intersection of the two trajectories. (For the reference sphere we choose $r = 1.2\,r_\star$, as for $r < 1.2\,r_\star$ rotation may be more or less rigid due to collisions. It can be shown that the choice of the radius has little influence on the results.) Those surface regions, where $\omega_L = \frac{e}{m}\,B\,\sin\delta \leq \omega_{L_0}$, are defined as wind bases (ω_{L_0} is a free parameter).[4]

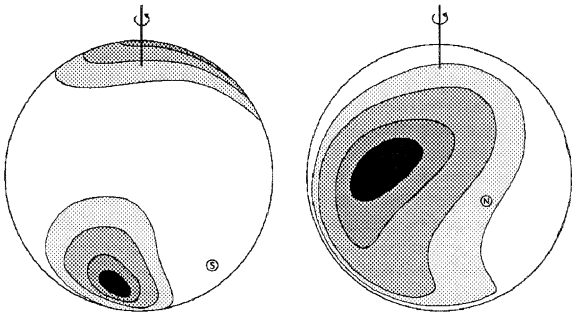

Fig. 8. Surface map of photospheric wind bases ($\omega_{L_0}{}' = const$) seen at phases $\Phi = 0.3$ (left panel) and $\Phi = 0.8$ (right panel). The rotation axis and magnetic poles (here a decentered dipole) are indicated.

In Fig. 8, contour lines for the normalized Larmor frequencies $\omega_{L_0}{}' = \frac{m\,\omega_{L_0}}{e\,B_p} = \frac{B}{B_p}\,\sin\delta = const$ (B_p is the field strength at the pole), with $\omega_{L_0}{}' = 0.1, 0.2, 0.3, 0.4$ (the inner dark region belongs to $\omega_{L_0}{}' = 0.1$) corresponding to $\delta = 6°, 12°, 18°, 24°$ are displayed for phases $\Phi = 0.3$ and 0.8. The wind flux increases from the shaded regions towards the dark regions. There appear two wind bases whose centers are located at $\Phi = 0.33$ and 0.85. These centers follow their respective magnetic poles, by roughly 30°, due to rotation. This result does not come unexpected: As the beam of photons is directed radially, the photons cannot transmit angular momentum to the absorbing wind particles which means that in case 2 (no magnetic field) the angular momentum is conserved along the wind trajectory (full drawn) until the "parking orbit" in the corotating cloud is reached and the access angular momentum is absorbed via collisions with the cloud particles. So only in the first quadrant ($0 \leq \theta \leq 90°$) (θ is the polar distance) and the third quadrant ($180 \leq \theta \leq 270°$) the wind can expand more or less freely along the magnetic field lines. On account of the conservation of angular momentum, however, this is forbidden for trajectories rising from the second ($90 < \theta < 180°$) and fourth quadrant ($270 < \theta < 90°$, ("angular momentum barrier", see Hunger et al. 1990).

The predicted wind bases agree with the observed bases ($\Phi = 0.3$ and 0.85, see Sect. 2.2). They also coincide with the maxima of the He equivalent widths ($\Phi = 0.35$ and 0.87)(see Fig. 11, upper right diagram). *Hence we conclude that He indeed is decoupled from the wind, leaving behind two He-patches.* In Sect. 5, we will use the contour lines $\omega_L{}' = \omega_{L_0}{}'$ to describe the observed phase variation of He I 4471.

The centers of the wind bases can also be estimated from the velocity law used (Kudritzki et al. 1989). For this law, the angle α between the radius vector and the tangent of trajectory 2 is given by $\tan\alpha = v_{\rm rot}/v_{\rm wind} \approx 0.5$, largely independent

[4] Alternatively, the component of the wind velocity v that is orthogonal to the magnetic field vector, $v_\perp = v\,\sin\delta$, or $v_\perp/v = \sin\delta < \sin\delta_0$ can be used as a criterion, as $\frac{1}{2}mv_\perp^2$ is the amount of kinetic energy that is converted into energy of rotation. Since B/B_p varies by less than a factor of 2, the two criteria are essentially identical.

of r. Assuming that trajectory 2 is parallel to trajectory 1 (ideal case), and taking the geometry of the dipole field, which implies $\tan\Theta = 2\tan\alpha$, i.e. $\tan\Theta \approx 1$, we get $\Theta \approx 45°$. (This result is only valid for a centered dipole with $\beta = 90°$ and for the plane of the rotational equator.) The polar distance of the wind base centers decreases with decreasing $v_{\rm rot}$. For zero rotation, the wind bases are centered at the poles.

4. Metal depletion

Metal depletion i.e. the decoupling of H from the metals, in addition to the decoupling of He from the metals thus leading to so called *run away metals* (see e.g. Springmann & Pauldrach 1992) could only occur at the border of the He-caps (large ω_L) where the density of the wind is too low to couple H. Since metal depletion is observed only in regions centered at the magnetic poles (irrespective of e/m and state of ionization/excitation, see e.g. Hunger et al. (1990)), and since no contour lines can be found which have their center of gravity at the poles, *it must be concluded that metal depletion cannot be induced (directly) by the stellar wind* (nor by diffusion, see Sect. 1).

So another agent must be sought for. In Fig. 9, the polar diagram of the u-magnitudes (Hesser et al. 1977) is reproduced. In this diagram, the length of the radius vector, measured from the stellar surface (dotted) to the solid line is proportional to the u-magnitude. The solid line, hence, reflects the phase distribution of $n_{0,2}$ H, i.e. the column density of neutral hydrogen in its second state of excitation. If one makes the (simplified) assumption that $n_{0,2}$ is constant, then the polar diagram yields the geometrical dimensions H of the hydrogen columns. We see the two corotating clouds (asymmetric due to the decentering of the dipole - see below). The clouds are located at the intersections of the magnetic and rotational equators (see also Groote & Hunger 1982). Accordingly, R.V. of the additional high quantum number Balmer lines (Groote & Hunger 1977) and $B_{\rm eff}$ of the decentered dipole vanish at the same phase (Fig. 9). [5]

But we also see two small clouds (cloudlets) above the magnetic poles. Since the large cloudlet follows the large corotating cloud, and vice versa, it is persuasive to assume that the cloudlets may consist of hydrogen and also of helium that has been reaccreted from the clouds. The clouds are assumed to contain matter of solar composition. This assumption follows from stationarity: matter from below the photosphere replenishing the mass lost in the wind is of solar composition – σ Ori E is believed to be a young star. The matter of the clouds and finally of the corona (see Sect. 6), hence, is also of solar composition (the transition between the two regimes is not selective). The probability of transition of the single He-ion from the photosphere to the clouds is reduced on account of the weak coupling between He^+ and metals. This reduction, however, is compensated by the large number density of photospheric He-ions in the wind

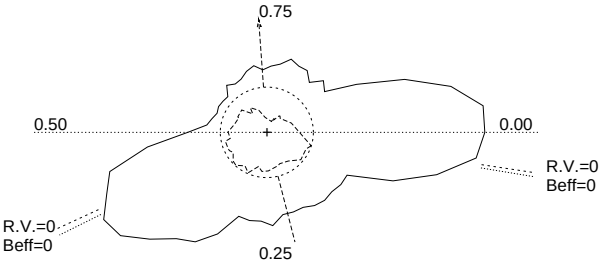

Fig. 9. Polar diagram of u-magnitude (full drawn, the length of the radius vector measured from the stellar surface (dotted) to the solid curve is proportional to the u-magnitude). It shows the two cloud absorptions, but also additional absorptions above the polar caps. The dashed curve inside the stellar circle describes the variations of the C IV resonance lines. C IV equivalent widths are proportional to the length of the radius vector measured from the center (+) to the dashed curve. They do not reproduce the symmetry of the clouds. The arrow (dashed) marks the axis of the (projected) decentered magnetic field.

bases. During the time the matter is stored in the clouds before it is released to the corona (which is of the order of one month – Groote & Hunger 1982), some of the hydrogen and helium atoms depending on the degree of ionization may migrate back to the stellar surface presumably towards the polar regions that follow the clouds, while metals are kept at large distances on account of the photon impact. [6]

The additional sources of opacity above the photosphere have the effect that all photospheric fluxes are weakened while profiles and equivalent widths remain unaffected, *as long as these sources are detached from the photosphere* (extinction due to an external absorber). This is the case for the corotating clouds. If the accretion scenario, however, is realistic one has to expect that a substantial fraction of the accreted matter reaches the photosphere. Thus the photosphere is stratified with a top layer of H (and He) (see also Sect. 5). If the optical depth of this layer is $\tau_{\rm H}$, one can show, by assuming an inverse Schuster-Schwarzschild model of line transfer that all spectral lines (except for H and He) will be weakened by the common factor $\approx e^{-\sqrt{3}\tau_{\rm H}}$. (The common factor averaged over the visible hemisphere is 0.6 which thus yields the optical depth of the Balmer bound-free (and free-free) continuum $\tau_H = 0.3$). This could explain the veiling of the absorption lines independent of e/m and state of ionization/excitation. In order to proof this scenario a detailed R.V. analysis of e.g. H_α would be important. Problems with the accretion scenario arise from the (partial) overlap of the wind bases with the accretion caps (see Fig. 10). In these regions we should expect two streams of matter, one upward and one downward which collide with (relative) velocities of several 100 km s^{-1}. This would lead to shocks and subsequent heating to temperatures of the order of 10^6 K, an effect

[5] The centers of the clouds, however, are shifted towards earlier phases ($\Delta\Phi = 0.04$, see also Groote & Hunger 1977) as the photospheric component of the u-magnitude of the star varies slightly with phase, because of the inhomogeneous surface distribution of He and H.

[6] Since the magnetic dipole is shifted towards north (see Table 2), the mean zenith distance of the field lines is greater at the S-pole than at the N-pole. Therefore the velocity of descent is expected to be smaller above the S-pole than above the N-pole which also would lead to a larger accumulation of H above the S-pole.

that could not remain unobserved since the optical depths of the shock regions presumably will be small. Therefore we conclude that the accretion rates must be much smaller than the mass loss rates and that the wind will probably inhibit accretion in the overlapping region (see darker gray region in Fig. 10).

5. Model calculations and surface mapping

In the preceeding sections it was shown that the centers of the observed wind bases and the observed He-patches coincide, thus giving strong support to the assumption of a fractionated stellar wind. The physics of the observed depletion of metals at the poles, however, is less clear and at present one can only guess that the depletion is due to the veiling by reaccreted H-atoms. In this section, it shall merely be checked whether the concept of H/He-fractionating leads to results that are consistent with the crucial observations of the phase distribution of the magnetic field, the equivalent widths of He 4471, and the equivalent widths of the UV resonance lines of C IV and Si IV (the latter appear strongly coupled to the magnetic field, in the sense that the equivalent widths vary inversely to the magnetic field).

Model calculations proceed as follows: The visible stellar disk at a given phase is divided in pixels of equal size (the number of pixels can be varied, here $\sim$ 1200 are used). For each pixel we calculate the corresponding area, the central R.V., and strength and direction of the magnetic field. Assuming different equivalent widths (or line profiles) in the belt-, wind- and accretion regions respectively, the surface integrated profiles and equivalent widths are calculated. This step is repeated for all phases (step width $\Delta\Phi$ = 0.05). For the magnetic field, given by the polar strength, its inclination angle β and the phase of the magnetic north pole $\Phi_{\rm N}$, a decentered dipole is assumed which may be decentered in all coordinates by $\Delta x, \Delta y, \Delta z$. (For σ Ori E it can be shown that the decentering in the three coordinates is necessary in order to account for the observations.) This decentering has large effects on the wind bases as the vectors of the magnetic field depend on it sensitively.

Given the magnetic field at the surface, the magnetic obliquity β and the rotation period P, the condition $\omega_L{}' \leq \omega_{L_0}{}'$ determines the surface regions (defined by the above described contour lines) where He is enriched. Furthermore, by assuming that accretion takes place only within circular caps at which the local field lines have a zenith distance $\leq \gamma_0$ (free parameter), then the metal deficiency caps are also defined. Accretion caps are calculated for $\gamma_0 = 9, 18, 27, 36°$. In (Fig. 10) only the case of $\gamma_0 = 27°$ is shown. Around the south pole (left panel) most zenith distances γ_0 are greater then 27°, while at the north pole (right panel), γ_0 is less then 9° in the circumpolar region. Hence, due to the shift of the dipole in the direction of the magnetic axis, the two polar caps have different dimensions, though one common value of γ_0 is used (see Table 2).

For σ Ori E ample observational data with sufficient phase coverage are available, namely the equivalent widths W_λ of He I 4471 (Hunger et al. 1989, Groote & Hunger 1977), W_λ of C IV 1548, 1551 and Si IV 1394, 1403, and the magnetic field

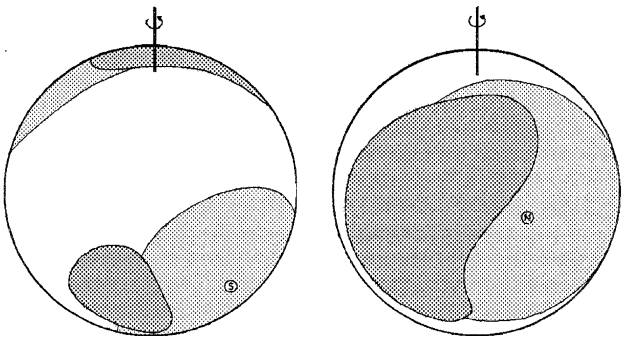

Fig. 10. The same as Fig. 8, but including the metal poor caps (light gray). At the south pole (left panel) most zenith distances γ_0 are greater then 27° inside the cap, while at the north pole (right panel), γ_0 is mostly less then 9° in the cap region.

$B_{\rm eff}$ (Bohlender 1993). Furthermore, the period $P = 1.19081 \pm 0.00001$ d is given (Hesser et al. 1977).

Before we discuss the results, some comments concerning the fit have to be made: W_λ of C IV and Si IV cannot be reproduced by full NLTE line formation analyses, in spite of considerable numerical effort invested (Rauch 1994). [7] LTE on the other hand yields profiles that are also not consistent with observations. The observed W_λ's of Si IV at the equatorial belt, where they should correspond to solar abundances (see Hunger et al. 1990) are too weak by a factor of 2, while W_λ's of C IV are too strong by a factor of 2. This discrepancy can hardly be ascribed to NLTE effects. It can be resolved if one assumes that near the magnetic equator the metals are stratified (see also below), with the abundances decreasing with height, as C IV 1548 is formed at $log\tau_{4000} = -0.6$, and Si IV 1394 at $log\tau_{4000} = -4.0$ (assuming LTE).[8]

So for the present analysis, we use the metal equivalent widths for belt, He-patches, and accretion caps as free parameters (W_λ = 1.33, 0.57, 0.18 Å for C IV and 1.51, 0.61, 0.88 Å for Si IV respectively.). Inside the polar caps, W_λ of the metal lines is drastically reduced (by at least a factor of 5, as the optical lines of C II and Si III suggest, Heber 1982). The surface integrated profiles, however, do not depend critically on the precise polar equivalent widths (W_λ = 0 could even be accepted) nor the law of interpolation applied for the transition from the belt to pole. [9]

[7] The paradox situation is that the more we approach LTE conditions, with decreasing $T_{\rm eff}$, the more difficult it is to obtain converged NLTE solutions. In order to compute the C IV line profiles one has to implement 5-6 model ions, from C to C^{5+}. Though only a minute fraction of C is in the C^{+++} state, small (relative) corrections in the densely populated C^{+} and C^{++} ions induce large (relative) corrections in the population of C^{+++}, and hence cooling rates which render the system unstable.

[8] Shore & Brown (1990) propose that the resonance lines of C IV and Si IV are formed in the clouds and in the (hypothetical) polar jets. The clouds, however, do not contribute substantially to the observed W_λ 's, as can be judged from the polar diagram of $W_{\lambda\,1548}(\Phi)$, Fig. 9.

[9] If one analyses strong and saturated lines which yield little information on radial velocities one is left with an ambiguity: large caps with

Table 2. Fit parameters of the surface model of σ Ori E.

i	=	54	± 2	[°]
β	=	70	± 3	[°]
Φ_N	=	0.725		
B_N	=	9650	± 300	[G]
Δx	=	0.09	± 0.03	R_*
Δy	=	0.09	± 0.03	R_*
Δz	=	0.09	± 0.03	R_*
v_{rot}	=	210		[km s^{-1}]
v_{wind}	=	420	± 100	[km s^{-1}]
$\omega_{L_0}{}'$	=	0.4	± 0.1	
γ_0	=	36	± 10	[°]

For the He-lines, we adopt $\varepsilon_{He} \approx 1$ (W_λ = 5.2 Å) for the centers of the He-patches, and $\varepsilon_{He} = 0.16$ (W_λ = 1.9 Å) outside the He-patches.

The obtained model parameters are listed in Table 2. The resulting model fits for B_{eff}, $W_{\lambda\,4471}$, $W_{\lambda\,1548}$, and $W_{\lambda\,1394}$ are shown in Fig. 11 as function of phase. Of all metal line equivalent widths, the contribution of the wind is eliminated by making use of the difference spectra, see above. The absolute scales, however, may contain systematic errors, due to the uncertainties of the continuum and unresolved blends. These amount to less then 20%. Curves reproduce the model fits and symbols with error bars the observations. For B_{eff}, two models are reproduced: a decentered dipole (full drawn) and a centered dipole (dotted). Preference is given to the former. The observations are well matched by the theory, except for phase Φ = 0.2 at which the observed W_λ 's of C IV display a rather deep and narrow minimum (this can also be seen at Fe III, Al III – see Hunger et al. 1990 – and less pronounced at Si IV). This minimum cannot be reproduced by any choice of parameters. A possible explanation would again be the assumption that the metals are stratified vertically near the poles in the manner as was proposed for the metal rich belt (see above). For as the S-pole crosses the line of sight (Φ = 0.2) close to the limb of the stellar disk, radiation emerges here at optical depths $\tau \approx 0.5$, while they are $\approx$ 1 for the N-pole (Φ = 0.75). If the metal abundances decrease with height, deep minima (per unit projected surface area) due to the center-limb variation, should be expected rather for the S-pole than for the N-pole.

A vertical stratification of metals in the polar regions would fit into the accretion scenario outlined in Sect. 4. Here a top layer of pure H was assumed for simplicity. However, this layer is expected to have a soft boundary at the bottom, which might lead to the postulated effect of stratification. The adopted W_λ 's for belt and polar caps (see above) also reflect the vertical stratification (see the depths of line formation, above). [10]

small underabundances yield practically the same phase variations as small caps with large underabundances. The ambiguity in the case of σ Ori E, however, is removed by the fact that the S-pole lies close to the rim (see Fig. 10, left panel). A small polar cap would not show up in the phase diagrams.

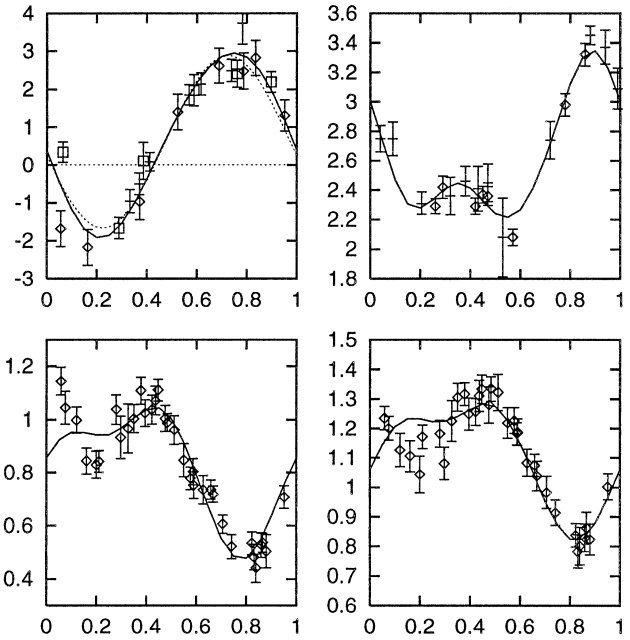

Fig. 11. Results of model fit (full drawn) as function of phase Φ: B_{eff} [kG] (upper left, dashed line corresponds to the centered dipole), W_λ [Å] of He I 4471 (upper right), W_λ [Å] of C IV 1548 (lower left), and W_λ [Å] of Si IV 1394 (lower right).

The surface parameters of σ Ori E presented in Table 2 agree largely with the model presented by Hunger & Groote (1992) which is based on the same observational material, however, on different assumptions concerning the wind bases. (Also, no observations concerning phase variations of the wind were available in 1992.) The determination of the wind bases required two more free parameter, and the wind bases had the shape of triangles. Due to the surface integration, however, the differences between the triangles and the present contour lines do not show up significantly in the phase diagrams.

6. Discussion

The aim of the presented paper was to test whether the concept of a fractionated stellar wind can explain the anomalous surface distribution of He and metals. A necessary first step was to check whether the wind is also distributed non-uniformly over the surface, a check that proved difficult on account of the low signal-to-noise ratio UV-spectrograms and also on account of the complex topology of the wind: the UV-resonance lines of C IV and Si IV revealed that the main wind component is phase independent and hence must be located outside the corotating clouds.

Since the verification of the phase dependent photospheric wind is the central issue we come back to Fig. 4a, and c that de-

[10] A similar vertical stratification of H and He is found in the He-weak variable HD 49333 (see Farthmann et al. 1994).

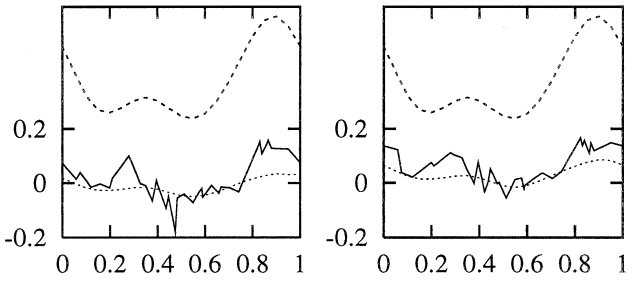

Fig. 12. Phase variations of wind absorption [Å] for C IV 1548 (left) and Si IV 1394 (right) $\Delta W_{\lambda/2}$(blue − red) (full drawn) compared to the He I 4471 variations (dashed, model calculations, scaled and shifted vertically). The dotted line, calculated in the same manner but with theoretical profiles, exhibits the influence of radial velocity shifts on the line profile due to the metal poor caps and also due to the He patches.

scribe the phase variations of the blue components of Si IV 1394 and C IV 1548. In Fig. 12, the difference $\Delta W_{\lambda/2}$(blue − red) is reproduced (full drawn, the zero point is arbitrary). In order to account for possible shifts stemming from radial velocity variations that are caused by the non-uniform surface distribution of the metals (and also of He - the latter may reduce the metal equivalent widths by a factor of up to 2), the respective differences $\Delta W_{\lambda/2}$ are computed for the final surface model of σ Ori E (with theoretical static profiles).

The result is shown in Fig. 12 (dotted). It demonstrates that the observed peaks indeed are caused predominantly by the wind and not by the Doppler effects of the surface patterns. (Note that the r.m.s. scatter of $\Delta W_{\lambda/2}$(blue − red) is less than 50 mÅ (wind regions excluded).) In the same diagram,the He I 4471 W_λ variations are plotted which are calculated likewise for the same surface model (dashed) but are scaled and shifted vertically for comparison. The phases of additional blue absorption (wind regions) lie closely to the phases of He line strength maxima and prove that wind bases and He patches indeed are identical.

This correlation is in contrast with the predictions of Michaud (1992), who shows that accumulation of He in the presence of wind can only occur where the wind is tuned down by the magnetic field to velocities that match the downward diffusion velocity of He. This assumption necessarily leads to two circumpolar He belts, in general, as the field strengths depend on the polar distances. Hence one should observe 4 peaks in the phase diagram of He (if the phase resolution is sufficient), which however is not observed in He variable stars, except for HD 37776 which is known to possess a quadrupole field configuration. However, Michaud (1992) does not consider rotation which on account of the "angular momentum barrier" shifts the wind bases from the poles to lower colatitudes (see Sect. 3). Instead of defining the diffusion areas by the magnetic colatitudes one has to use the contour lines, as shown in Fig. 8. For a critical (large) value of $\omega_{L_0}{}'$, the conditions for diffusion can be reached, i.e. He-enrichment via diffusion can take place at the surface. This will occur in more or less broad belts which are defined by two contour lines located outside the here postulated wind bases and which, hence, surround the He-patches. From the phase variation of W_λ He 4471 one can infer that the diffusion area probably covers a major fraction of the surface between the two He-patches. This region should be expected to be enriched in He following Michaud (1992). This enrichment indeed is observed: In Sect. 5 it is stated that the surface mapping procedure requires $\varepsilon_{He} = 0.16$ outside the He-patches which is about twice as solar. This otherwise unexplained observation seems to confirm Michaud's theory as applied to σ Ori E.[11]

The discussion shows that we deal with two distinctly different mechanisms that may cause enrichment of He:

1. The decoupling of He in the fractionated wind which implies (local) mass loss rates of the order $10^{-10}\mathrm{M}_\odot\mathrm{yr}^{-1}$, and
2. classical diffusion which seems to imply rates of the order of $\leq 10^{-13}\mathrm{M}_\odot\mathrm{yr}^{-1}$.

The former leads to He-enrichment of the order of $\varepsilon_{\mathrm{He}} \approx 1$, and the latter $\varepsilon_{\mathrm{He}} \approx 0.2$ (σ Ori E).

Now let us discuss the mass loss rate of σ Ori E: Direct empirical determination of the photospheric wind seems to be hardly possible on account of the complex topology of the wind (magnetic field, rotation, clouds, corona). This also applies to the theory of radiatively driven wind when applied to σ Ori E. However, there is some hope that the mass loss rate can eventually be determined from the coronal wind which for reasons of continuity must be equal to that of the photospheric wind. The existence of a hot gas beyond $r = 6\,r_\star$ is postulated by Havnes & Goertz (1984). A stellar wind emerging from the stellar photosphere continually feeds the two corotating clouds which are trapped by the strong magnetic field, until the density of the cloud matter has reached the critical limit at which it no longer can be contained by the magnetic field. Field lines reconnect and transfer their energy to the released matter. This happens at the Alfvenic points of both clouds, at time intervals that are determined by the stellar mass loss rate. So the picture is that there are two hot spots, nearly oppositely located, that circle the star at about 6 stellar radii, each within 29 hours. The initial plasma torus rapidly expands into a corona. According to Havnes & Goertz (1984), coronal temperatures of $T = 10^5 - 10^7$ K are attained. These high temperatures and energies are confirmed by observations of X-rays (Berghöfer & Schmitt 1994), and by relativistic electrons which become manifest by radio emission (Drake et al. 1987). The coronal wind reaches velocities of up to 600 km s^{-1}. If the state of ionization of C and Si were known, one would be able to derive the mass loss rate due to the coronal wind. Hence at present we can only estimate the mass loss rate: $\log \frac{\dot{M}}{\mathrm{M}_\odot\mathrm{yr}^{-1}} = -10 \pm 1$. This estimate is based on Hamann's (1981) evaluation and considers that only 20 % of the total wind profile of C IV 1548 is due to the photospheric wind.

[11] Vauclair et al. (1991) also studied diffusion in non-rotating A_p and B_p stars with the result that He will accumulate at the magnetic poles, when the mass loss rate is approximately solar. Adding rotation, one would probably come to the same conclusion as in Michaud's theory, as a small effective mass loss rate corresponds to a large Larmor frequency ω_L for a star with otherwise $\dot{M} \approx 10^{-10}\mathrm{M}_\odot\mathrm{yr}^{-1}$. Likewise, the diffusion area is shifted away from the poles.

7. Conclusions

σ Ori E is the first example of a star with a fractionated stellar wind, i.e. a wind whose chemical composition is distinctly different from the composition of its base. The class of stars with fractionated winds is expected to be small, because the conditions are narrow: not only $T_{\rm eff}$ is restricted ($T_{\rm eff}$ defines the density of the wind), but also the state of ionization of He. For, if He were doubly ionized in the wind base of σ Ori E, it would even be more closely coupled to the metals than H and segregation could not occur (Springmann & Pauldrach 1992). There are a few candidates (He-variables) that have to be probed, but none of them with such complete coverage of observations.

Decoupling of He may also occur on the surface of stars which do not have a magnetic field and/or do not rotate, whenever the above named presumably narrow conditions are fulfilled. An excellent candidate for the case "no magnetic field, no rotation" appears to be the exotic object HD 144941 in which hydrogen and metals are reduced by (nearly) the same factor, namely 1.6 dex for H and 1.7 $\pm$ 0.2 dex for each of the seven analysed metals (Harrison & Jeffery 1996). The effective temperature is T = 23200 K and the gravity log g = 3.9. These parameters are essentially the same as for σ Ori E (Hunger et al. 1989).

Decoupling of He *and* H (*run away* metals) is not observed in the photosphere of σ Ori E. Metal depletion at the poles may be a secondary effect of the wind, in that some of the trailing H (and He) atoms are reaccreted at the opposite polar cap. The latter scenario, though, meets with some problems, for there may be domains near the surface where accretion and wind overlap which may lead to shock fronts. The latter have not been observed so far.

Acknowledgements. We gratefully acknowledge the discussions with Drs. U. Springmann, A. Pauldrach, and J. Puls concerning fractionated winds, and with Dr. M. Schüßler and Prof. D. Schlüter concerning rotating magnetospheres. Our main thanks go to Prof. U. Heber who in all phases of this paper contributed substantially to the results by comments, criticism and LTE calculations. Our thanks go also to Drs. T. Rauch and U. Leuenhagen who computed model atmospheres and line profiles in static and expanding NLTE atmospheres. We are greatly indebted to Prof. D. Reimers for critically reading the manuscript and for valuable comments. Likewise, we are indebted to our referee, Dr. J.D. Landstreet, for his constructive criticism and valuable suggestions which undoubtedly added substance to the paper. Last not least we want to thank Drs. S.J. Adelman and P. Barker for the painstaking efforts of obtaining phase covering IUE observations, without them this paper would have been incomplete.

References

Abbott D.C. 1982, ApJ, 259,282
Babel J. 1995, A&A (in press)
Barker P.K., Brown D.N., Bolton C.T., Landstreet J.D. 1982, in Advances in Ultraviolet Astronomy: Four Years of IUE Research, eds. Y. Kondo, J.M. Mead, R.D. Chapman (NASA CP-2238), p.589
Berghöfer T.W. & Schmitt J.H.M.M. 1994, A&A, 290, 435
Bohlender D.A. 1988, Thesis, The University of Western Ontario, London, Ontario
Bohlender D.A. 1993, IAU Symp. 162, Antibes Juan Les Pins, eds. A. Balona et al., p.155
Bohlender D.A., Brown D.N., Landstreet J.D., Thompson I.B. 1987, ApJ, 323, 325
Drake S.A., Abbot D.C., Bastian D.S., Bieging J.H., Churchwell E., Dulk G., Linsky J.L. 1987, ApJ 322, 902
Farthmann M., Dreizler S., Heber U., Hunger K. 1994, A&A, 291, 919
Groote D., Hunger K. 1976, A&A, 52, 303
Groote D., Hunger K. 1977, A&A, 56, 129
Groote D., Hunger K. 1982, A&A, 116, 64
Hamann W.R. 1981, private communication
Harrison P.M., Jeffery C.S. 1996 (submitted to A&A)
Havnes O., Goertz C.K. 1984, A&A, 138, 421
Heber U. 1982, private communication
Hesser J.E., Moreno H., Ugarte P. 1977, ApJ, 216, L31
Hunger K., Heber U., Groote D. 1989, A&A, 224, 57
Hunger K., Heber U., Groote D. 1990, in properties of Hot Luminous Stars, Boulder-Munich Workshop, ed. C.D. Garmany, p.307
Hunger K., Groote D., Heber U. 1991, in Evolution of Stars: The Photospheric Abundance Connection, eds. G. Michaud and A. Tutukov, IAU, p.173
Hunger K., Groote, D. 1992, in Peculiar Versus Normal Phenomena in A-Type and Related Stars, IAU Coll. 138, eds. M.M. Dworetsky, F. Castelli, R. Farragiana, p.394
Kemp J.C., Herman L.C. 1977, ApJ, 218, 770
Kudritzki R., Pauldrach A., Puls J., Abbot D.C. 1989, A&A 219, 205
Landstreet J.D., Borra E.F. 1978, ApJ, 224, L5
Mégessier C. 1984, A&A, 138, 267
Michaud G., Duprés J., Fontaine G., Montmarle T. 1987, ApJ 322, 302
Michaud G. 1992, in The atmospheres of Early-Type Stars, eds. U. Heber and C.S. Jeffery, Lecture Notes in Physics 401, 189
Pauldrach A. 1989, private communication
Pedersen H. 1979, A&AS, 35, 313
Rauch T. 1994, private communication
Shore S.N., Adelman S.J. 1981, in Upper Main Sequence Chemically Peculiar Stars, 23rd Liège Astrophys. Coll., p.429
Shore S.N., Brown D.N. 1990, ApJ, 365, 665
Springmann U.W.E., Pauldrach A.W.A. 1992, A&A 262, 515
Vauclair S., Dolez N., Gough D.O. 1991, A&A 252, 618
Walborn N.R., Hesser J.E. 1976, ApJ, 205, L87

This article was processed by the author using Springer-Verlag LaTeX A&A style file *L-AA* version 3.